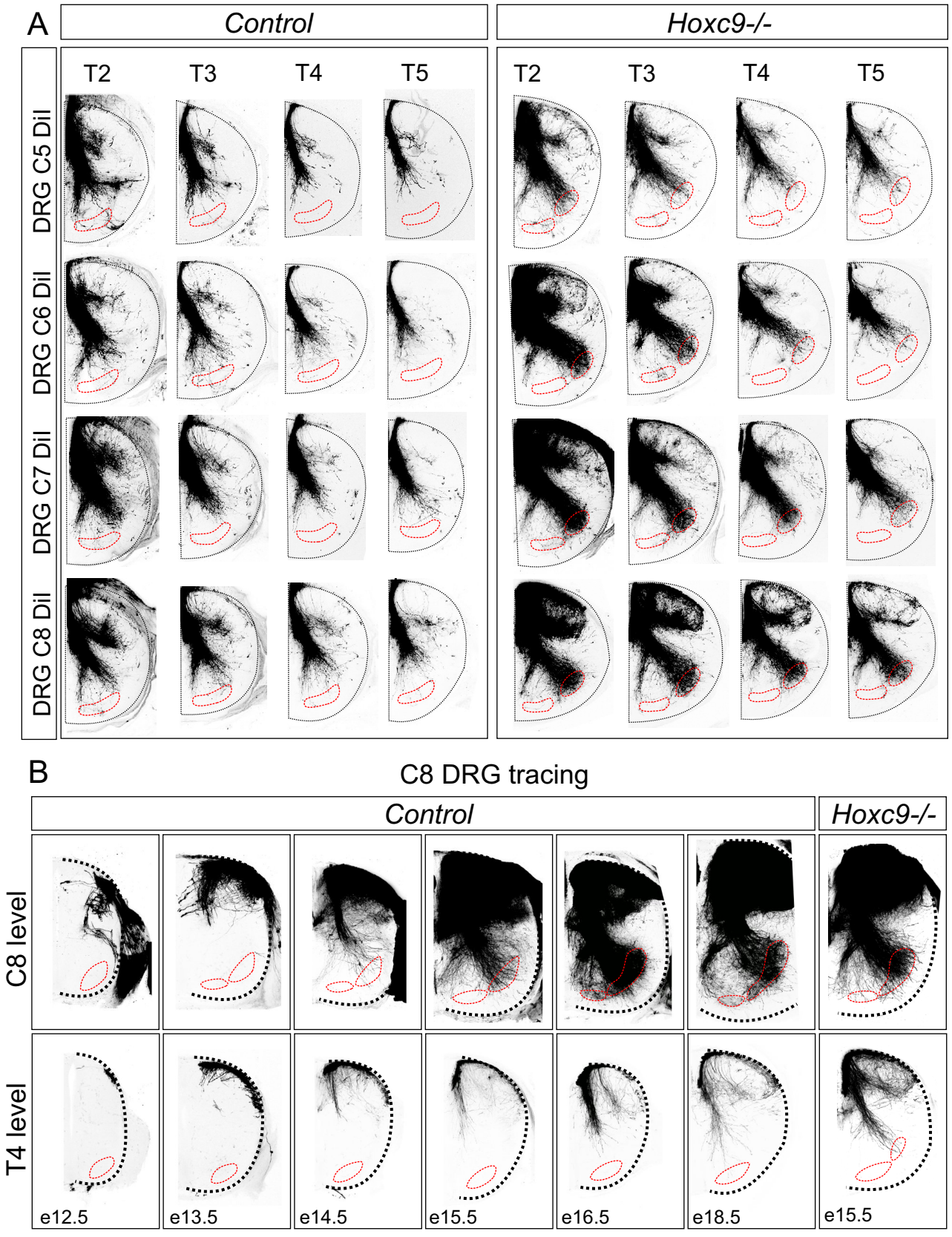
A
Control
Hoxc9-/-
T2
T3
T4
T5
DRG C5 DiI
DRG C6 DiI
DRG C7 DiI
DRG C8 DiI
B
C8 DRG tracing
Control
Hoxc9-/-
C8 level
T4 level
e12.5
e13.5
e14.5
e15.5
e16.5
e18.5
e15.5

Figure S1. Sensory Neuron Afferent Projections in Control and *Hoxc9* Mutants. **Related to Figure 1.**
(A) DiI tracing from indicated cervical DRG (C5, C6, C7, and C8) showing sensory afferent projections in thoracic segments (T2-T5) of control and *Hoxc9-/-* mice at P0. Segmental positions are shown at top. Approximate position of MNs is outlined in red. In *Hoxc9* mutants, sensory projections extend to the more laterally positioned ectopic LMC neurons.
(B) DiI tracing of C8 DRG sensory projections analyzed at segmental levels C8 and T4 at indicated stages of development. Panels on far right show tracing from C8 at e15.5 in *Hoxc9-/-* mice. In *Hoxc9* mutants, C8-derived sensory neurons extend towards T4-level MNs beginning at e15.5

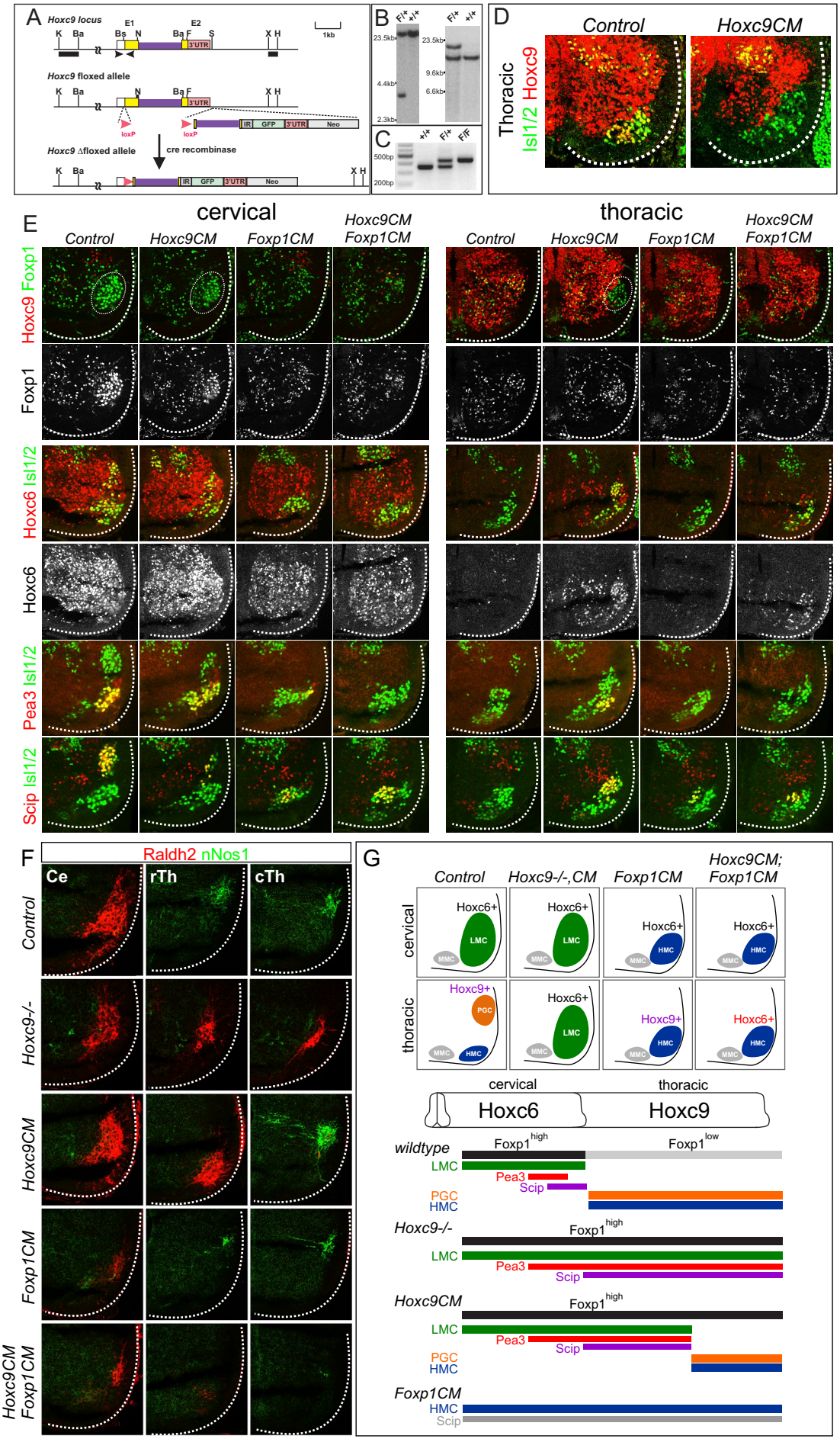
A
Hoxc9 locus
E1
E2
K Ba Bs N Ba F S X H
1kb
3'UTR
Hoxc9 floxed allele
loxP
loxP
IR GFP 3'UTR Neo
Hoxc9 Δfloxed allele
cre recombinase
B
23.5kb
4.4kb
2.3kb
9.6kb
6.6kb
C
500bp
200bp
D
Control
Hoxc9CM
Thoracic
Isl1/2 Hoxc9
E
cervical
thoracic
Control
Hoxc9CM
Foxp1CM
Hoxc9CM Foxp1CM
Hoxc9 Foxp1
Foxp1
Hoxc6 Isl1/2
Hoxc6
Pea3 Isl1/2
Scip Isl1/2
F
Raldh2 nNos1
Ce
rTh
cTh
Control
Hoxc9-/-
Hoxc9CM
Foxp1CM
Hoxc9CM Foxp1CM
G
Control
Hoxc9-/-,CM
Foxp1CM
Hoxc9CM; Foxp1CM
cervical
thoracic
Hoxc6+
Hoxc9+
LMC
HMC
PGC
MMC
Hoxc6
Hoxc9
wildtype
Foxp1high
Foxp1low
Pea3
Scip
Hoxc9-/-
Hoxc9CM
Foxp1CM

Figure S2. Analysis of MN Subtypes in *Hoxc9-/-*, *Hoxc9CM* and *Hoxc9;Foxp1* Mutants. Related to Figure 2.
(A) Schematic of *Hoxc9* genomic locus and targeting strategy. E1, Exon1; E2, Exon2; yellow boxes, coding regions; purple lines, introns; pink boxes, 3´ untranslated regions (UTRs). Black boxes, Southern blot probes in (B). Black arrowheads, PCR primers in (C). The targeting construct contains ~10kb genomic DNA from the 5´ BamHI site to the 3´ XbaI site. IR, internal ribosome reentry site; GFP, eGFP reporter; Neo, pgk-neo cassette. Restriction enzyme sites: Ba, BamHI; Bs, BspMI; F, FokI; H, HindII; K, KasI; N, NaeI; S, StuI; X, XbaI.
(B) Southern blot analyses. Left, genomic DNA digested with SphI, 357bp XbaI-HindIII probe, >24kb wild-type (+) and ~3.2kb targeted bands (F); right, genomic DNA digested with BglII, 772bp KasI-BamHI probe, ~13kb wild-type (+) and ~20kb targeted bands (F).
(C) PCR reactions on genomic DNA using Hoxc9 lox5 and Hoxc9 5R primers. ~350bp band, wild type allele (+); ~430bp band, targeted allele (F).
(D) Analysis of e13.5 thoracic spinal cord showing loss of Hoxc9 protein in MNs of $Hoxc9^{CM}$ mice. Hoxc9 expression is lost in a subset of ventral interneurons, but retained in most dorsal non-MN populations.
(E) Expression of Foxp1, Hoxc6, Hoxc9, Pea3 and Scip in indicated mouse lines at cervical and thoracic levels at e13.5. $Foxp1^{+}$ LMC neurons are circled for clarity. In both $Hoxc9^{CM}$ and $Hoxc9^{CM}$; $Foxp1^{CM}$ mice, Hoxc6 is derepressed at thoracic levels. In $Foxp1^{CM}$ and $Hoxc9^{CM}$; $Foxp1^{CM}$ mice, Pea3 expression is lost from MNs, whereas Scip is ectopically expressed at both cervical and thoracic levels.
(F) Expression of the LMC marker Raldh2 and thoracic PGC marker nNos in the indicated mouse mutants. Sections are from cervical and thoracic spinal cord at e13.5. Expression of markers is shown at cervical (Ce), rostral thoracic (rTh), and caudal thoracic (cTh) levels. In $Hoxc9^{CM}$; $Foxp1^{CM}$ mice, no ectopic Raldh2 expression is observed in thoracic segments. In $Hoxc9^{CM}$ mice PGC identity is retained in cTh segments.
(G) Schematic summary of MN phenotypes in control, *Hoxc9-/-*, $Hoxc9^{CM}$, $Foxp1^{CM}$, and $Hoxc9^{CM}$; $Foxp1^{CM}$ mice. Grey shading of Scip expression in $Foxp1^{CM}$ mice indicates non-LMC pool subtype expression.

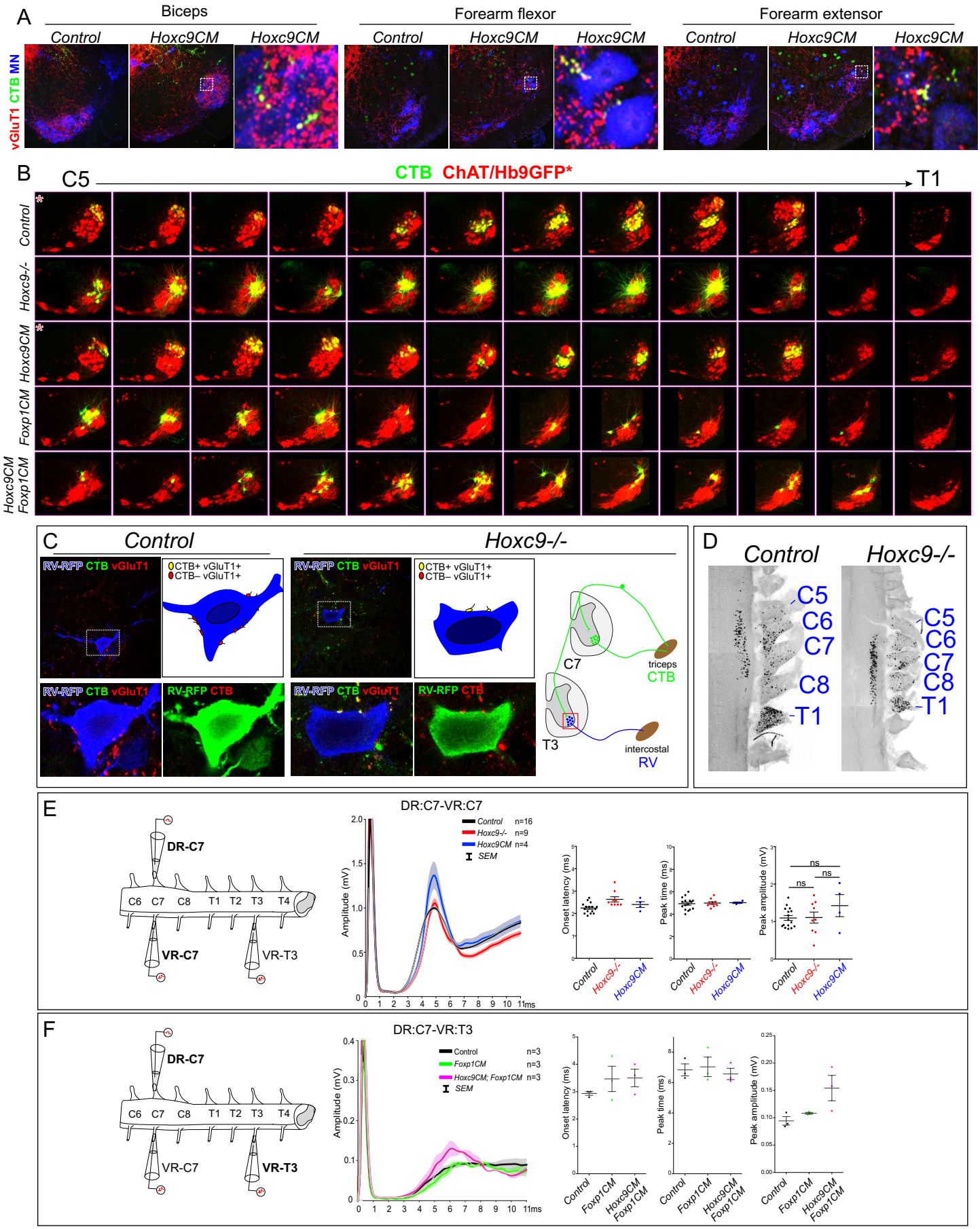
A
Biceps
Forearm flexor
Forearm extensor
Control
Hoxc9CM
Hoxc9CM
vGluT1 CTB MN
B
C5
CTB ChAT/Hb9GFP*
T1
Control
Hoxc9-/-
Hoxc9CM
Foxp1CM
Hoxc9CM
Foxp1CM
C
Control
Hoxc9-/-
RV-RFP CTB vGluT1
CTB+ vGluT1+
CTB– vGluT1+
RV-RFP CTB
C7
triceps
CTB
T3
intercostal
RV
D
Control
Hoxc9-/-
C5
C6
C7
C8
T1
E
DR:C7-VR:C7
DR-C7
C6 C7 C8 T1 T2 T3 T4
VR-C7
VR-T3
Control n=16
Hoxc9-/- n=9
Hoxc9CM n=4
SEM
Amplitude (mV)
11ms
Onset latency (ms)
Peak time (ms)
Peak amplitude (mV)
ns
Control
Hoxc9-/-
Hoxc9CM
F
DR:C7-VR:T3
DR-C7
C6 C7 C8 T1 T2 T3 T4
VR-C7
VR-T3
Control n=3
Foxp1CM n=3
Hoxc9CM; Foxp1CM n=3
SEM
Amplitude (mV)
11ms
Onset latency (ms)
Peak time (ms)
Peak amplitude (mV)
Control
Foxp1CM
Hoxc9CM Foxp1CM

Figure S3. Analysis of Sensory-Motor Connectivity in *Hoxc9* and *Foxp1* Mutant Mice. Related to Figure 3.
(A) Tracing of sensory synapses onto MNs after intramuscular injections into indicated muscles. Because of their small size, for distal flexors and extensors multiple muscles were injected. Synapses between sensory neurons of limb muscles and thoracic MNs are observed in *Hoxc9CM* mice. For biceps and forearm flexors, MNs are labeled with ChAT, for distal limb extensors, *Hb9::GFP* was used in conjunction with ChAT antibody staining.
(B) Retrograde labeling of the triceps MN pool after intramuscular injection of CTB in the indicated mouse mutants. MNs were labeled through co-detection of ChAT and GFP in an *Hb9::GFP* background. Triceps motor pool position is restricted to segments C5-T1 in *Hoxc9* mutant mice. In the *Foxp1* mutant background the triceps pool clustering is disrupted, but still confined to cervical segments.
(C) Thoracic MNs targeting intercostal MNs receive triceps sensory input in *Hoxc9-/-* mice. Rabies virus (RV)-RFP was injected into rostral intercostal muscles while CTB was injected into triceps. Mice were injected at P3 and examined at P5.
(D) Labeling of MNs and pSNs after tracer injections into triceps muscle. Images show whole mount spinal cords with DRG attached at P5 in control and *Hoxc9-/-* mice.
(E) Schematic of setup for dorsal root stimulation and ventral root recordings is shown on the left. Traces from indicated mouse lines measured from ventral root (VR) at C7 after dorsal root (DR) C7 stimulation. Lines show mean values ± SEM (lighter shading). Number of mice analyzed is indicated in graph. Quantification of onset latencies, peak times, and peak amplitudes in DR:C7-VR:C7 recordings. Bars show mean values ±SEM.
(F) Ventral root recordings at T3 after C7 dorsal root stimulation in $Hoxc9^{CM}$, $Foxp1^{CM}$ mice. Traces show ventral root recordings upon C7 dorsal root stimulation in indicated mouse lines. Quantification of onset latencies, peak times, and peak amplitudes in DR:C7-VR:T3 recordings. Bars show mean values ±SEM.

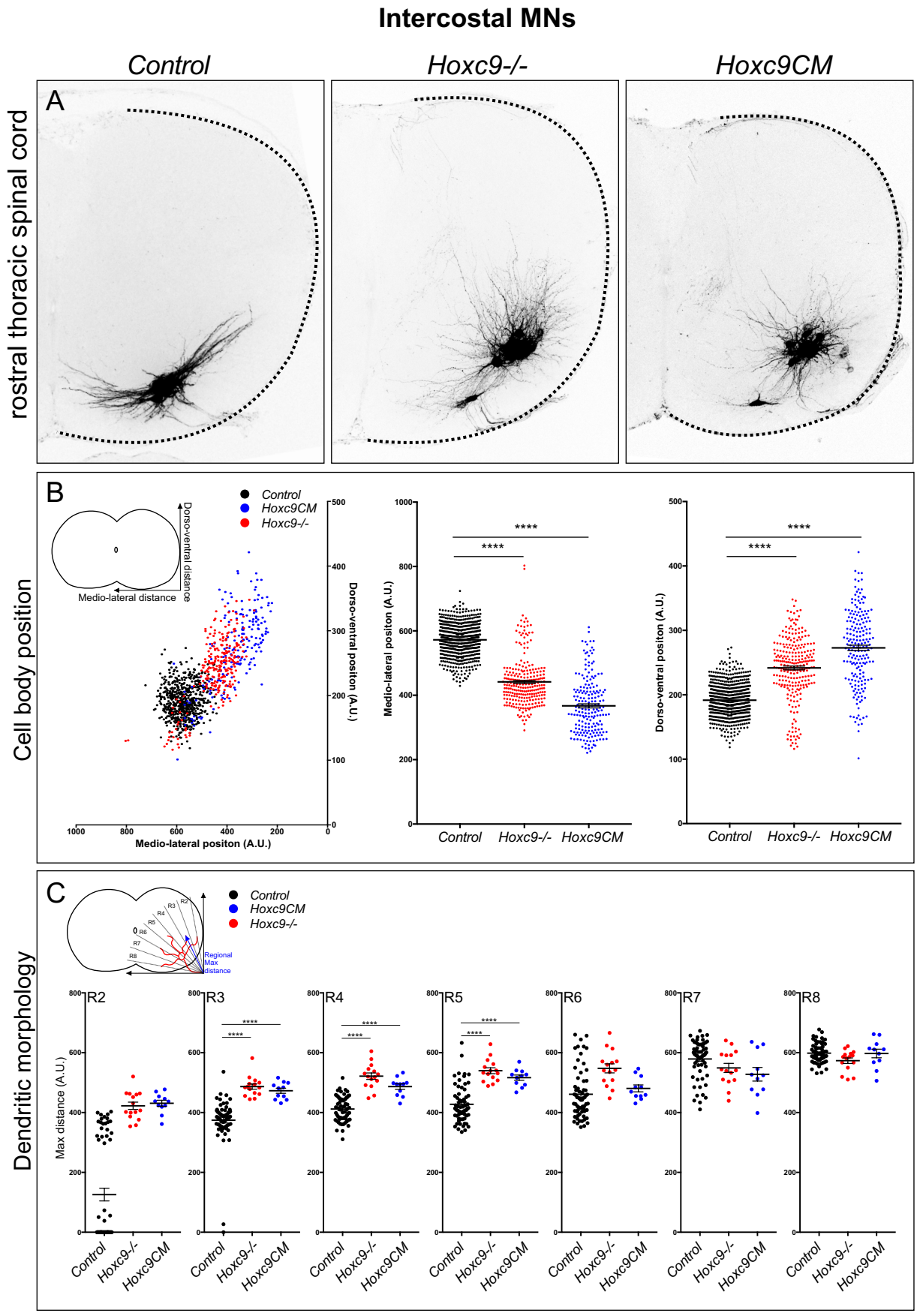
Intercostal MNs
Control
Hoxc9-/-
Hoxc9CM
A
rostral thoracic spinal cord
B
Cell body position
Control
Hoxc9CM
Hoxc9-/-
Dorso-ventral distance
Medio-lateral distance
Dorso-ventral positon (A.U.)
Medio-lateral positon (A.U.)
****
C
Dendritic morphology
Regional Max distance
R2
R3
R4
R5
R6
R7
R8
Max distance (A.U.)

Figure S4. Intercostal MN Position and Dendritic Morphology in *Hoxc9* Mutants. Related to Figure 4.
(A-C) Rostral thoracic intercostal MNs were traced by injection of rhodamine dextran into intercostal muscles.
(A) Representative images of intercostal MNs at the rostral thoracic regions in control, *Hoxc9-/-*, and $Hoxc9^{CM}$ mice.
(B) Quantification of MN soma positions in control and *Hoxc9* mutants. Schematic of distance measurement is shown (top-left). Distances are normalized by the dimensions of the spinal cord. Cell body positions are mapped on an X-Y plot (left panel; X axis, medio-lateral position; Y axis, dorso-ventral position). Quantification of the medio-lateral (middle panel) and dorso-ventral (right panel) cell body positions. In *Hoxc9* mutants, cell bodies are shifted dorso-laterally. Total number of cells: control, n=630 cells, 7 mice; $Hoxc9^{CM}$, n=194 cells, 2 mice; *Hoxc9-/-*, n=254 cells, 2 mice. ****$p<0.0001$; Bars on the scatter plots show mean±SEM.
(C) Quantification of dendritic morphologies in control and *Hoxc9* mutants. Schematic of distance measurement is shown (top-left). Spinal cord is divided into 9 regions (10 degrees separation between each). Maximum distance is taken from each region. Distances are normalized by dimensions of the spinal cord. Each plot shows quantification for each region (from region (R)2 to R8). Total number of samples: control, n=64 sections (150µm), 7mice; $Hoxc9^{CM}$, n=11 sections (150µm), 2mice; *Hoxc9-/-*, n=15 sections (150µm), 2mice. ****$p<0.0001$; Bars on the scatter plots show mean±SEM.

Supplemental Experimental Procedures

Conditional Targeting of the *Hoxc9* locus

Mouse strains used in this study include *Foxp1flox* (Surmeli et al., 2011), *Olig2::Cre* (Dessaud et al., 2007), and *Hoxc9-/-* (McIntyre et al., 2007). To generate *Hoxc9* conditional targeting constructs, a 65bp fragment containing a *LoxP* sequence was cloned into a BspMI site located 74bp 5´ to the translation start site within the *Hoxc9* exon 1. The following sequences were then inserted into a StuI site (3´ to the two known polyadenylation sites) of the *Hoxc9* locus: a second *LoxP* site followed by a ~1.8kb NaeI-BamHI fragment containing a *Hoxc9* intron, an IRES-eGFP fragment, a ~1kb FokI-StuI fragment containing the 3' UTR of *Hoxc9*, polyadenylation sequences from the bovine albumin gene, and a pgk-neo cassette for positive selection. The final targeting construct was assembled in a pMoluc vector (Feng et al., 2002): it contains a ~10kb BamHI-XbaI *Hoxc9* genomic region with the modifications mentioned above. The homologous sequences at the 5´ and the 3´ arms are ~4.2kb and ~2.2kb, respectively. The targeting construct was linearized at the SfiI site (located in the vector's multiple cloning sites, 5´ to the 5´ arm) and electroporated into W9.5 ES cells as described (Dragatsis et al., 2000). ES cells with the targeted allele were first verified by Southern blot analyses (see below) and then injected into C57B/6J blastocysts using standard procedures (Bradley, 1987). Male chimeras were crossed with C57B/6J females to generate heterozygous offspring.

Genotypes were confirmed first by Southern blot analyses: SphI-digested genomic DNA was hybridized with a 357bp 3´-flanking XbaI-HindIII fragment probe. BglII-digested genomic DNA was hybridized with a 772bp 5´-flanking KasI-BamHI fragment probe. PCR genotyping was performed with the following primer pairs: floxed *Hoxc9* allele primers, Hoxc9lox5 (5'-CCTTGGGTCCAGAGTTGC-3'), Hoxc95R (5'-CCTGGACGCTAGGAGGTC-3'); Dfloxed *Hoxc9* allele primers, Hoxc9lox5, mHoxc9IR (5'-CTTCTCAGACCTTCCTGC-3').

Ventral Root Recordings

P6 mice were anesthetized by incubating on ice for 5 min. Anesthetized pups were decapitated and the spinal cords were isolated under ice-cold artificial cerebrospinal fluid (dissection aCSF: 128.35mM NaCl, 4mM KCl, 0.58mM NaH_2PO_4, 21mM $NaHCO_3$, 30mM D-Glucose, 1mM $CaCl_2$, and 3mM $MgSO_4$; oxygenated with carbogen ($95\%O_2/5\%CO_2$). The hemisected spinal cords were then transferred to a customized recording chamber and incubated for 30 min. in the chamber, which was perfused continuously with artificial cerebrospinal fluid (recording aCSF: 128.35mM NaCl, 4mM KCl, 0.58mM NaH_2PO_4, 21mM $NaHCO_3$, 30mM D-Glucose, 2mM $CaCl_2$, and 1mM $MgSO_4$; oxygenated with carbogen ($95\%O_2/5\%CO_2$) with a speed of 5ml/min.

Extracellular recordings were obtained from ventral roots (C7 and T3) in response to stimuli (duration, 0.2ms; interval, 30s) from a dorsal root C7 (Differential AC Amplifier 1700, A-M Systems; amplified at 1000X, acquired with 1 Hz low pass and 1 kHz high pass filters) and fed to an A/D interface (Digidata 1550 digitizer, Molecular Devices; sampled at 10 kHz). Data was analyzed with Clampfit (v10, Molecular Devices). Stimulation signals were delivered using a stimulus isolator (A365, WPI). In order to determine the stimulation intensity, dorsal roots were stimulated with increasing intensities (0-30μA) and a minimum intensity giving the maximum response was chosen. For the recording, dorsal roots were stimulated with a 1.5X minimum intensity (18-45μA).

Off-line analysis was performed by averaging 10 to 15 traces. The onset latency of the afferent-evoked ventral root potentials was defined by a time from a stimulation artifact at which a first measurable deflection of the potential from the baseline was observed. The peak time points were determined by a time-point when a maximum-amplitude was reached within 10ms from a stimulation artifact.

Viral Tracing

P5 mouse pups were anesthetized by a hypothermia, in which pups were incubated on ice for 4 min. Pups were transferred to an ice filled stage, and a small incision was made on the skin, followed by removal of underlying muscles except intercostal muscles. 1:1 mixtures of AAV virus and Rabies virus were mixed with 1/10 volume of 1% FastGreen. ~0.4μl of virus mixtures were injected into the target muscles using a syringe needle (1701SN, 30°/33 gauge, 9.52mm long, Hamilton). Injection volume was controlled using a dispenser (PB600-1 Repeating Dispenser, Hamilton). After injection, the incision was sealed with several drops of Vetbond (3M). Pups were waken by incubating in a warm incubator and returned to a mother mouse. After 8 days, spinal cords were isolated by the following steps: First, pups were anesthetized by the injection of a lethal dose of Ketamine (200mg/kg) and Xylazine (20mg/kg) mixtures into the intraperitoneal cavity. Next, pups were perfused with 10ml cold PBS for

2min, followed by a perfusion with 50ml cold PFA for 8min. Last, isolated spinal cords were pinned down on a sylgard plate and postfixed for 6hr in a cold room.

Plotting of Premotor Populations

40μm cryosection slices were immunostained with RFP, vGluT1, and ChAT antibodies. Images were acquired with Olympus confocal microscope (FV1000) at 4X. X-Y coordinates for labeled premotor cell bodies indicated in μm units were determined using TRAKEM in Fiji. Isoline plots were generated from the X-Y scatter plots using kde2d in Matlab, in which bivariate gaussian kernel distribution was used with a constant number of 6 isolines as described (Botev et al., 2010). The color of the isolines was set automatically by Matlab such that the yellow line represents the highest density in each plot and the color could represent different values between plots. In each plot, the areas encircled by the same color isoline have the same cell density.

Supplemental References

Botev, Z.I., Grotowski, J.F., and Kroese, D.P. (2010). Kernel Density Estimation Via Diffusion. Ann Stat *38*, 2916-2957.

Bradley, A. (1987). Production and analysis of chimeric mice. In Teratocarcinomas and Embryonic Stem Cells: A Practical Approach, E.J. Robertson, ed. (Oxford: IRL Press), pp. 131-151.

Dessaud, E., Yang, L.L., Hill, K., Cox, B., Ulloa, F., Ribeiro, A., Mynett, A., Novitch, B.G., and Briscoe, J. (2007). Interpretation of the sonic hedgehog morphogen gradient by a temporal adaptation mechanism. Nature *450*, 717-720.

Dragatsis, I., Levine, M.S., and Zeitlin, S. (2000). Inactivation of Hdh in the brain and testis results in progressive neurodegeneration and sterility in mice. Nat Genet *26*, 300-306.

Feng, T., Li, Z., Jiang, W., Breyer, B., Zhou, L., Cheng, H., Haydon, R.C., Ishikawa, A., Joudeh, M.A., and He, T.C. (2002). Increased efficiency of cloning large DNA fragments using a lower copy number plasmid. Biotechniques *32*, 992.

McIntyre, D.C., Rakshit, S., Yallowitz, A.R., Loken, L., Jeannotte, L., Capecchi, M.R., and Wellik, D.M. (2007). Hox patterning of the vertebrate rib cage. Development *134*, 2981-2989.

Surmeli, G., Akay, T., Ippolito, G.C., Tucker, P.W., and Jessell, T.M. (2011). Patterns of spinal sensory-motor connectivity prescribed by a dorsoventral positional template. Cell *147*, 653-665.